Photocrosslinking of human telomeric G-quadruplex loops by *anti* cyclobutane thymine dimer formation

Dian G. T. Su[a], Huafeng Fang[a], Michael L. Gross[a], and John-Stephen A. Taylor[a,1]

[a]Department of Chemistry, Washington University, St. Louis, MO 63130

Edited by Philip C. Hanawalt, Stanford University, Stanford, CA, and approved June 8, 2009 (received for review March 4, 2009)

The unusual structural forms of telomere DNA, which protect the ends of chromosomes during replication, may render it vulnerable to unprecedented photodamage, possibly involving nonadjacent bases that are made proximate by folding. The G-quadruplex for the human telomere sequence consisting of a repeating d(TTAGGG) is one unusual form. Tel22, d[AGGG(TTAGGG)$_3$], forms a basket structure in the presence of Na^+ and may form multiple equilibrating structures in the presence of K^+ with hybrid-type structures predominating. UVB irradiation of d[AGGG(TTAGGG)$_3$] in the presence of Na^+ results in a *cis,syn* thymine dimer between two adjacent Ts in a TTA loop and a mixture of nonadjacent *anti* thymine dimers between various loops. Irradiation in the presence of K^+, however, produces, in addition to these same products, a large amount of specific *anti* thymine dimers formed between either T in loop 1 and the central T in loop 3. These latter species were not observed in the presence of Na^+. Interloop-specific *anti* thymine dimers are incompatible with hybrid-type structures, but could arise from a chair or basket-type structure or from triplex intermediates involved in interconverting these structures. If these unique nonadjacent *anti* thymine dimer photoproducts also form in vivo, they would constitute a previously unrecognized type of DNA photodamage that may interfere with telomere replication and present a unique challenge to DNA repair. Furthermore, these unusual *anti* photoproducts may be used to establish the presence of G-quadruplex or quadruplex-like structures in vivo.

mass spectrometry | photochemistry | nonadjacent dimer | DNA | UV

Telomeres are repetitive sequences at the ends of chromosomes that function in concert with telomerase and a number of other proteins to protect the ends of chromosomes from shortening during successive rounds of replication (1–3). The human telomere sequence consists of repeating d(TTAGGG) that may fold into various repeating G-quadruplex structures. Short fragments of the human telomere sequence can exist in a myriad of structures that depend on their sequence and on the cations present (4–7). To date, basket (8, 9), parallel (10), and (3 + 1) structures including hybrid-1 and hybrid-2 (11–14) type G-quadruplex forms have been determined by NMR and crystallography. The oligodeoxynucleotide, d[AGGG(TTAGGG)$_3$] (Tel22), adopts a basket structure in solutions containing Na^+ (8), whereas in the presence of K^+, the predominant intracellular cation, the hybrid-type structures are favored over the basket (11, 13) and/or chair (15) structures (Fig. 1).

Recently, we discovered that a highly unusual interstrand-type nonadjacent, *anti* thymine photodimer (Fig. 2*B*), previously only found in dried or ethanolic solutions of UVC irradiated DNA (16), can form in aqueous solution. Irradiation of d(GTATCATGAGGTGC) with UVB light produced a high yield of *cis,anti* thymine photodimer between T2 and T7 under slightly acidic conditions (17). This *anti* photodimer must originate from some folded structure, still unknown, that brings T2 in a head to tail arrangement with T7 followed by photoinduced [2 + 2] cycloaddition reaction between the two 5, 6 double bonds. An important implication of this observation is that *anti* thymine photodimers might also form in G-quadruplex forms of human telomeric DNA. Among the various G-quadruplex structures that could lead to *anti* thymine photodimers are the basket and chair structures, which have two lateral TTA loops in close proximity. Other structures, such as the parallel and hybrid structures do not have proximate loops, suggesting that photochemical reactions such as this may be developed as structural probes even in vivo.

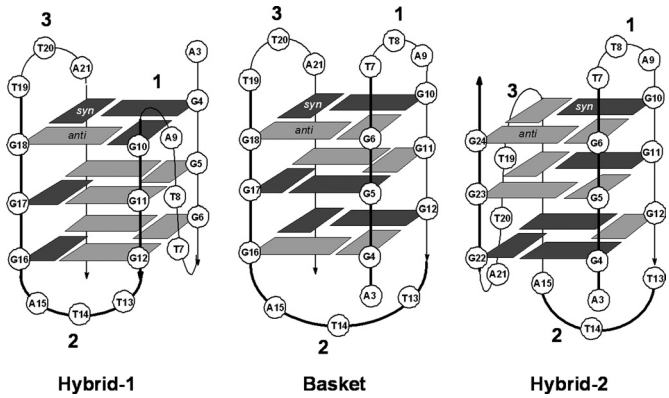

Fig. 1. Known basket, hybrid-1, and hybrid-2 triple quartet forms of human telomeric DNA that could be adopted by Tel22. The numbering system for the bases starts from 1 in the human telomere sequence d(TTAGGG)$_n$. The loops are numbered sequentially, and dark and light gray boxes represent *syn* and *anti* guanines, respectively.

To our knowledge, the photochemistry of native human telomeric DNA has never been investigated, although the photoinduced hydrogen abstraction reactions of iodouracil substituted telomeric DNA has been reported (18). In 1989, however, Cech and coworkers did report the formation of crosslinks upon 254 nm irradiation of the folded form of the closely related *Oxytricha*, d$(T_4G_4)_4$, and *Tetrahymena* d$(T_2G_4)_4$ telomeric sequences as evidence for a G-quartet structure (19). The photocrosslinks formed in the presence of Na^+ were found to occur primarily between T11 and T27 in d$(T_4G_4)_4$ and between T1 or G3 and T13 in d$(T_2G_4)_4$ by gel electrophoresis of chemical cleavage products, and were ascribed to G-quartet chair structures. The structures of the photoproducts involved in the crosslinking, however, were never determined. Herein, we report that irradiation of G-quadruplex forms of the human telomeric sequence d[AGGG(TTAGGG)$_3$] (Tel22) with biologically relevant UVB light (280–320 nm) and in the presence of the biologically relevant cation K^+ results in a significant amount of *anti* thymine dimers between either T in loop 1 with the central

Author contributions: D.G.T.S. and J.-S.A.T. designed research; D.G.T.S. and H.F. performed research; M.L.G. contributed new reagents/analytic tools; D.G.T.S., M.L.G., and J.-S.A.T. analyzed data; and D.G.T.S., M.L.G., and J.-S.A.T. wrote the paper.

The authors declare no conflict of interest.

This article is a PNAS Direct Submission.

[1]To whom correspondence should be addressed. E-mail: taylor@wustl.edu.

This article contains supporting information online at www.pnas.org/cgi/content/full/0902386106/DCSupplemental.

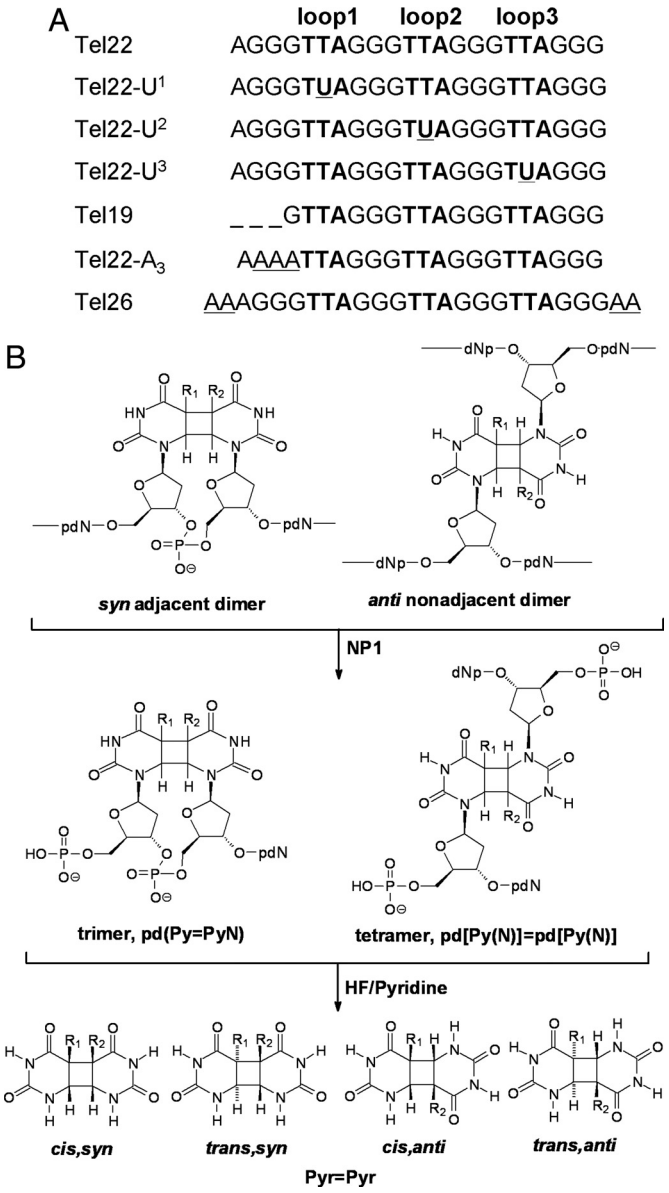

Fig. 2. Telomeric substrates and cyclobutane pyrimidine dimer photoproducts. (*A*) Telomeric sequences used in the present work. The superscript *n* in U^n (n = 1, 2, and 3, respectively) refers to the loop in which the second T was replaced by U. (*B*) Adjacent and nonadjacent photoproducts and their nuclease P1 (NP1) digestion products and HF/pyridine hydrolysis products. R = CH_3 for thymine, and R = H for uracil. *Trans,syn* and *cis,anti* pyrimidine dimers exist as enantiomeric pairs.

T in loop 3. We also discuss the mechanistic and biological implications of these findings.

Results and Discussion

To determine whether nonadjacent photoproducts can be produced in the G-quadruplex forms of the human telomere, we analyzed the irradiation products of the 22-mer fragment, d[AGGG(TTAGGG)$_3$] (Tel22) and its derivatives by an enzyme-coupled mass spectrometry assay (17, 20). This 22-mer fragment was initially chosen because it adopts the basket form in Na^+ solution (8), which was expected to lead to efficient photocrosslinking between loops 1 and 3. To determine which nucleotides were involved in photoproduct formation, we substituted various Ts with Us, which have the same photochemical and base pairing properties but differ in mass.

Formation and Irradiation of Telomeric G-Quadruplexes. To prepare the G-quadruplexes, ODNs were first denatured and then either cooled quickly or slowly to 0 °C with similar results, which is consistent with a rapid rate of folding (21). The circular dichroism (CD) spectra of Tel22 in Na^+ and K^+ closely matched previously reported spectra (*SI Text* and Fig. S1). ODNs in which a U was substituted for a T (Fig. 2*A*) gave similar CD spectra to those of Tel22. Samples were then irradiated on ice with UVB light for 2–2.5 h.

Polyacrylamide Gel Electrophoresis (PAGE) of Irradiation Products. Analysis of ^{32}P-end-labeled Tel22 irradiation samples by denaturing PAGE revealed the presence of two major bands I and II (Fig. 3*A*). Band I has the same mobility as Tel22, whereas band II had increased mobility, suggesting that altered structures had formed. Most significantly, the rate of formation of band II was greater with K^+ than with Na^+ and is opposite to what had been previously observed for $d(T_4G_4)_4$ and $d(T_2G_4)_4$ (19).

Electrospray Ionization-Mass Spectrometry (ESI-MS) of Irradiation Products. For mass spectrometry studies, we submitted nonradiolabeled Tel22 to the same procedure as described above. The individual bands were visualized by brief exposure to UVC light and excised from the gel. The products from irradiation in K^+ solution for 2 h were extracted from bands corresponding to I and II, and from the intervening band. ESI-MS analysis of these products on a quadrupole time-of-flight (Q-Tof) mass spectrometer gave a molecular weight of 6,966, as did those from the unirradiated parent ODN, indicating that they are intramolecular photoproducts.

Nuclease P1 (NP1)-Coupled HPLC Assay of Irradiation Products. NP1 is an endonuclease that degrades photoproduct-containing DNA to smaller photoproduct-containing fragments that are characteristic of the type of photodamage (20, 22). NP1 functions by binding to the base portion of a nucleotide after which it hydrolyzes the phosphodiester bond on the 3′-side to yield a deoxynucleotide with a 3′-hydroxyl group (23, 24). Because NP1 does not bind to photodimerized bases, it cannot cut on the 3′-side of either nucleotide involved in photodimer formation. As a result, NP1 digestion produces trinucleotides, pd(T=TN), from adjacent thymine dimers, and tetranucleotides, pd[T(N)]=pd[T(N)], from nonadjacent dimers, and mononucleotides, pdN, from undamaged nucleotides (Fig. 2*B*) (17, 20). With our HPLC method, mononucleotides elute before 20 min, trinucleotides from 20 to 35 min, and tetranucleotides from 35 to 45 min, as confirmed by ESI-MS analysis of the eluents. HPLC analysis of the NP1 digestion products of Tel22 irradiated in Na^+ solution showed a sharp peak corresponding to an adjacent dimer and a small broad peak corresponding to nonadjacent thymine dimers (Fig. 4*A*). Analysis of the irradiation products in the presence of K^+, however, showed numerous additional sharp peaks corresponding to nonadjacent thymine dimers (Fig. 4*B*).

DNA sequences with a folded secondary structure have increased mobility in gel electrophoresis compared with the unfolded structure (19, 25–27). NP1 digestion and mass spectral analysis of the faster moving band II corresponding to a species formed in K^+ solution showed tetranucleotides (peaks 7, 8, 9, 10, and 11) as the major products (Fig. 3*B*). The higher mobility also indicates formation of photodimers that crosslink the DNA into loops, thereby increasing the mobility relative to that of the unmodified ODN. The NP1 digestion products of the intermediate band contained a mixture of trinucleotides (peaks 2 and 3) and tetranucleotides (peaks 7, 8, 9, 10, and 11). NP1 digestion and analysis of band I (Fig. 3*B*), however, revealed the presence of only trinucleotides (peaks 2 and 3), indicative of adjacent thymine dimers, which would not be expected to change the mobility of the oligodeoxynucleotides, as was observed.

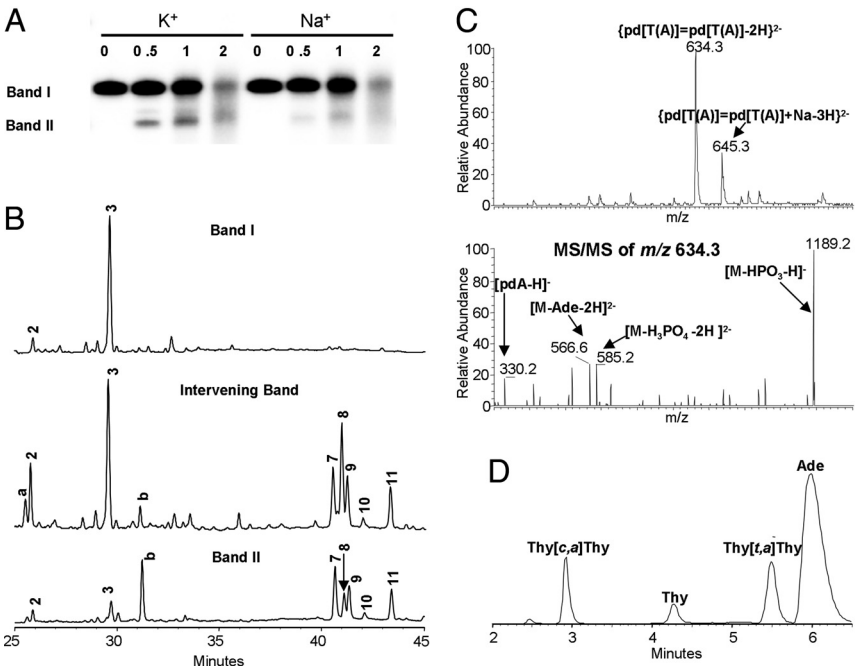

Fig. 3. Analysis of UVB irradiated telomeric quadruplexes. (*A*) Tel22 was UVB irradiated in 150 mM Na^+ or K^+ solution at pH 7.5 for the number of hours indicated in the lane headings, ^{32}P-end-labeled, and then subjected to 15% denaturing PAGE. Bands I and II and the intervening band were excised and subjected to NP1 digestion. (*B*) NP1-coupled HPLC assay of nonradiolabeled samples corresponding to bands I, II, and the intervening band. HPLC peaks a and b were not observed in nonelectrophoresed samples and could not be assigned. Products were detected at 260 nm where the nondimerized bases have their maximum absorption. (*C*) Mass spectra and product-ion mass spectra of the major nonadjacent photoproduct HPLC peak 8. The observation of $[pdA - H]^-$ and $[M - Ade - 2H]^{2-}$ indicate that adenine is the nonphotodimerized base. (*D*) HPLC assay of HF/pyridine hydrolysis products of HPLC peak 8 that was contaminated with adjacent peaks. The hydrolysis products were detected at 205 nm where the photodimers have their maximum absorbance, and their stereochemistry assigned by correlation with authentic thymine photodimers (Fig. S2*B*). The small thymine peak may be caused by the decomposition of thymine *anti* dimers in the course of hydrolysis (17). Analysis of various HPLC fractions established peak 8 to be the *trans,anti* photodimer.

Nucleotide Composition of the Trimer and Tetramer NP1 Degradation Products. We separated the NP1 degradation products by HPLC and determined their nucleotide compositions by ESI-MS and MS/MS analysis. The nucleotides were identified first by their molecular weight deduced from the MS and second by tandem mass spectrometry (MS/MS) experiments. For example, those nucleobases that were not involved in dimer formation were cleaved from the parent ion upon collisional activation. Thus, HPLC peak 3 was assigned to pd(T=TA) because it gives a molecular ion $[M - H]^-$ at *m/z* 938.2 and a characteristic product ion $[M - Ade - H]^-$ at *m/z* 803.1 (Fig. S2*A*). We also detected a small amount of the TA* photoproduct (peak 2) (Fig. S3*B*) (28, 29). HPLC peaks 7 and 8 were both assigned as isomeric pd[T(A)]=pd[T(A)] on the basis of a molecular ion $[M - 2H]^{2-}$ at *m/z* 634.3 and characteristic product ions $[pdA - H]^-$ at *m/z* 330.1 and $[M - Ade - 2H]^{2-}$ at *m/z* 566.6 (Fig. 3*C*). Using similar reasoning, we assigned HPLC peak 11 to pd[T(T)]=pd[T(A)] (Fig. S4*A*). Some peaks appeared to be contaminated with products from flanking peaks and were assigned to the major component, whereas others appeared to contain two products (Table 1).

Stereochemistry of the Thymine Photodimers. The stereochemistry of the thymine photodimers was assigned by comparing the base portion of the photoproducts with authentic thymine cyclobutane dimers (17, 30, 31) (Fig. S2*B*). The base portion of the photodimers was obtained by treating the trinucleotides and tetranucleotides with 70% hydrogen fluoride in pyridine (HF/pyridine) (Fig. 2*B*). HPLC peak 3 was thereby determined to correspond to the *cis,syn* thymine photodimer (Fig. S2 *B* and *C*), and peaks 7, 8, 9, 10, and 11 to thymine photodimers of either *cis,anti* or *trans,anti* stereochemistry or both (Fig. 3*D*, Fig. S5*B*, Fig. S4*B*, and Table 1). The *syn* stereochemistry is consistent with photodimer formation between adjacent thymines, whereas the *anti* stereochemistry is expected for photodimer formation between thymines in opposing loops (interstrand-type product) (Fig. 2*B*) (17). More *cis,anti* and *trans,anti* products were detected than expected based on their symmetry properties (1 *t,a* and two *c,a* for pd[T(A)]=pd[T(A)] suggesting that there may be additional isomers because of restricted rotation.

Mapping of Thymine Photodimer Sites. Because the ODN sequence is repetitive, it is not possible to identify directly the specific thymines involved in adjacent and nonadjacent thymine photodimer formation by analysis of the trinucleotide and tetranucleotide degradation products. To solve this problem, we labeled the various loops by constructing three telomere sequences Tel22-U^n (n = 1, 2, and 3), in which the second T in the TTA loop n was replaced with U, which undergoes the same photodimerization as T but lacks a C5 methyl group (Fig. 2). Owing to the substrate specificity of NP1, the second pyrimidine is always retained in the trimeric digestion products of an adjacent pyrimidine dimer formed within a single loop, and in the tetrameric digestion products of a photodimer formed between two different loops. Thus, if a pyrimidine photodimerization takes place within or between a loop containing a U, the tri- and tetranucleotide digestion products will have different HPLC retention times, and the molecular ions will be 14 u lower than those only involving loops containing only Ts. Furthermore, analysis of the characteristic product ions in the ESI-product-ion spectra can establish whether the U is involved in the photodimerization.

Irradiation of Tel22-U^2 in K^+ followed by NP1 digestion resulted in a nearly identical set of photoproducts as that from

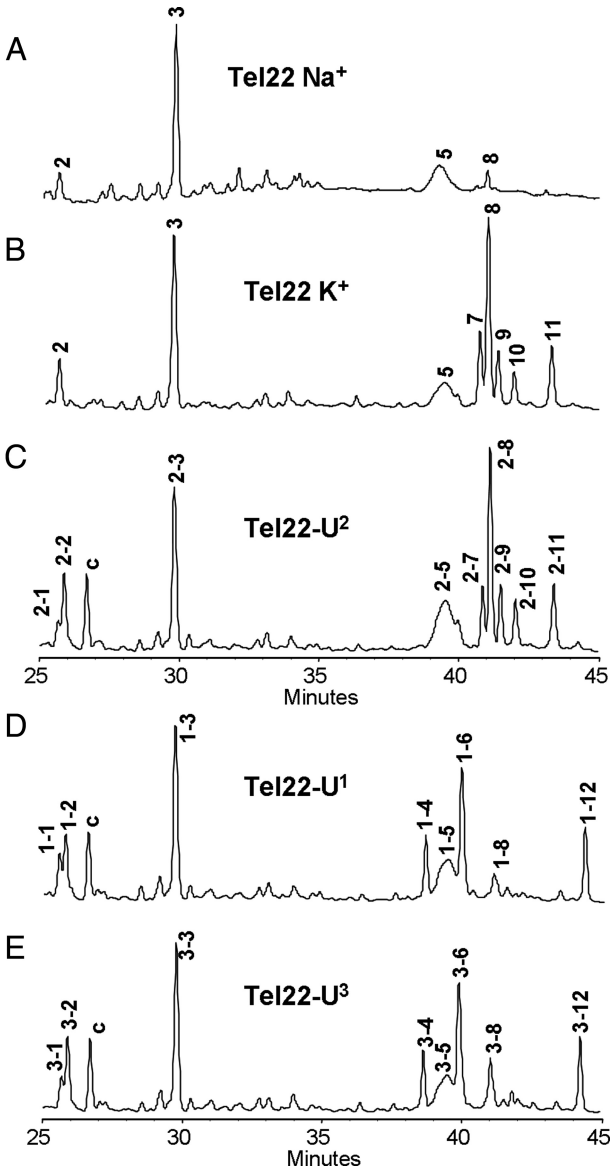

Fig. 4. NP1-coupled HPLC assay of Tel22 and the U-substituted sequences after 2.5 h UVB irradiation at pH 7.5. (*A*) Tel22 in 150 mM Na^+ solution. (*B*) Tel22 in 150 mM K^+ solution. (*C–E*) Tel22-U^n in 150 mM K^+ solution. The HPLC peaks are labeled n-m, in which n refers to the loop that is substituted by U, and m refers to the order of elution. Peak c could not be assigned. Peaks 1–3 are trinucleotides resulting from adjacent photoproducts, and peaks 4–12 are tetranucleotides resulting from nonadjacent photoproducts.

Tel22, with the exception of a photoproduct (HPLC peak 2-1, Fig. 4*C*), which was identified as pd(T=UA) (Fig. S3*A*). This sole U-containing product indicates that the Ts in loop 2 do not photodimerize with Ts in the other 2 loops. In contrast, irradiation and digestion of both Tel22-U^1 and Tel22-U^3 led to HPLC peaks, *n*-1, *n*-4, *n*-6, and *n*-12 (*n*=1 and 3, respectively, where *n* refers to the loop containing the U) (Fig. 4 *D* and *E*). These peaks corresponded to the same photoproducts found in Tel22 except that a T was replaced by a U. The results clearly establish the involvement of loops 1 and 3 in thymine photodimerization, and furthermore, that both Ts of loop 1 photodimerize preferentially with only the second T of loop 3. The basis for the latter conclusion is that Tel22-U^1 yielded primarily pd[T^1(U)]=pd[T^3(A)] and pd[U^1(A)]=pd[T^3(A)] (Fig. S6), whereas Tel22-U^3 gave primarily pd[T^1(T)]=pd[U^3(A)] and pd[T^1(A)]=pd[U^3(A)] (Fig. S7). The detailed assignment of photoproducts of Tel-U^n is given in Table S1.

Table 1. Stereochemistry, base composition, and loop assignment of the NP1 digestion products of UV-irradiated Tel22 shown in Fig. 4*B*

HPLC peak	Stereochemistry	Base composition
2	—	T=AG*
3	*c,s*†	T=TA
5	*c,a*	T(T)=T(A) T(A)=T(A)
7	*c,a*‡	T^1(A)=T^3(A)
8	*t,a*‡	T^1(A)=T^3(A)
9	*c,a*§	T^1(A)=T^3(A)
10	*c,a and t,a*¶	T^1(T)=T^3(A) T^1(A)=T^3(A)
11	*t,a*‖	T^1(T)=T^3(A)

The superscripted number a or b in the NP1 digestion product T^a(X)=T^b(Y) refers to the loop from which the T arose based on the results of uracil substitution.
*Product-ion spectrum shown in Fig. S3*B*.
†Product-ion spectrum and hydrolysis products shown in Fig. S2.
‡Product-ion spectrum and hydrolysis products shown in Fig. 3 *C* and *D*.
§Product-ion spectrum and hydrolysis products shown in Fig. S5.
¶Could not be assigned to a specific product
‖Product-ion spectrum and hydrolysis products shown in Fig. S4.

It is noteworthy that we observed a broad HPLC peak in the digestion products of irradiated Tel22 (peak 5), and the sequences substituted with U (peaks 1–5, 2–5, and 3–5), whether irradiated in Na^+ or K^+ solution (Fig. 4). Analysis of this peak indicates that it corresponds to a mixture of thymine photodimers between different pairs of loops (Table S1). We speculate that some or all of these photoproducts are not produced from specific G-quadruplex structures but from a small fraction of nonspecifically folded isomers that exist in equilibrium with these structures.

Mechanistic Implications. The inefficient formation of *anti* thymine photodimers in the Na^+ form of Tel22, which has a basket structure with two proximate lateral loops (8) (Fig. 1), was unexpected. Even more unexpected was the efficient formation of *anti* thymine photodimers between loops 1 and 3 in the K^+ form of Tel22, which is thought to exist primarily in hybrid-1 and/or hybrid-2 conformations that lack proximate loops (11, 13). These hybrid structures, however, are also thought to be in dynamic equilibrium with either or both basket and chair conformations (11, 13, 15) that have proximate lateral loops that could photocrosslink (Figs. 1 and 5). Given that the basket form which Tel22 adopts in Na^+ did not facilitate photocrosslinking between loops 1 and 3, it is unlikely that the basket form in K^+ would be any better. It is possible, however, that interloop photodimer formation would be more favorable in the chair form, which has an antiparallel arrangement of loops 1 and 3 compared with the parallel arrangement in the basket form. The higher preference for isomeric pd[T(A)]=pd[T(A)] products (peaks 7 and 8) (16% yield) over isomeric pd[T(T)]=pd[T(A)] products (6.5% yield), is in agreement with a report that the Ts and As involved in the chair conformation can form a T-A-T-A quartet (32).

Another explanation for the enhanced photocrosslinking in K^+ comes from the recent discovery that the closely related 22-mer human telomeric sequence d[$(GGGTTA)_3$GGGT] adopts a different basket structure (Form III) with K^+ (9) than the one found with Na^+ (8) (Fig. 5). The Form III basket structure corresponds to the Na^+ basket structure in which the first GGG sequence misaligns to disrupt the first G quartet and

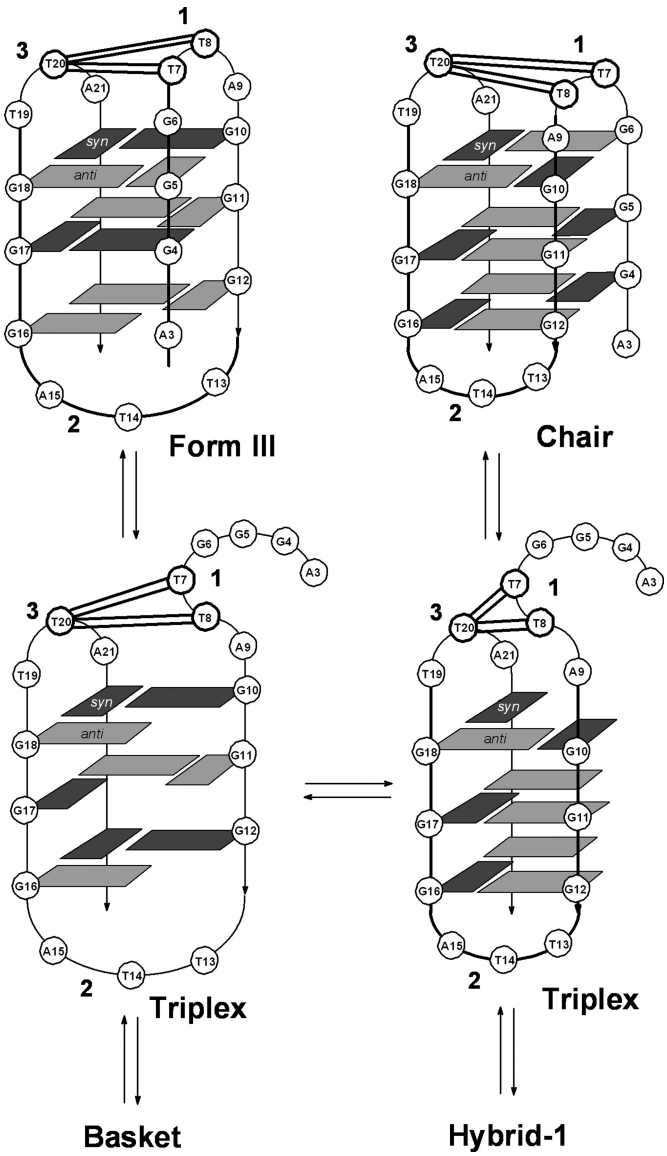

Fig. 5. Photodimer sites mapped onto chair and Form III G-quadruplex forms of Tel22 and onto triplex intermediates possibly involved in equilibrating between these and other structures. Solid double lines indicate sites of observed *anti* thymine photodimer formation between loops 1 and 3.

to increase the size of the first loop by one nucleotide. The increased size of loop 1 in the Form III structure in K^+ is expected to better facilitate photodimer formation between loop 1 and loop 3 than the basket structure formed in Na^+. In support of this, the *Oxytricha* telomeric sequence $d(T_4G_4)_4$, which adopts a basket structure with two 4-nucleotide loops in Na^+ (33), photocrosslinks efficiently between the third T in loop 1 and the third T in loop 3 (19).

A third possibility is that the triplex intermediates involved in interconverting the various quadruplex structures (11, 34, 35) can themselves facilitate *anti* thymine dimer formation, and are more accessible and/or stable in K^+ than in Na^+. To test whether triplexes might be involved, we prepared a truncated form of Tel22, Tel19 (Fig. 2*A*), that lacks the first three Gs necessary to complete the fourth strand of the quadruplex and, thus, limits the structure to intermediate triplex forms. Deleting the 3 Gs or replacing them with As in Tel22-A_3 (Fig. 2*A*) resulted in comparable amounts of the same *anti* thymine dimers as formed in Tel22 (Fig. S8 *A* and *B*, respectively), except that the relative yields of isomeric *cis,anti* and *trans,anti* pd[T(A)]=pd[T(A)] (peaks 7 and 8) were greatly diminished. These results show that although formation of *anti* thymine photodimers between loops 1 and 3 can presumably proceed through intermediate G-quadruplex-like triplex structures, they are not produced in the same relative yields as observed for the G-quadruplex form of Tel22.

To determine whether or not photocrosslinking between loops 1 and 3 could be suppressed by choosing a sequence known to more greatly favor a hybrid structure, we investigated the photochemistry of Tel26, d[AAA$(GGGTTA)_3$GGGAA]. This sequence was found by NMR to initially adopt a mixture of hybrid-1 and -2 structures in K^+ that quantitatively converts to the hybrid-1 structure on incubation (11, 13). Even though the hybrid-1 structure lacks proximate loops, the overall yield of *anti* thymine photodimers in Tel26 was nearly the same as was found for Tel22, except that there was an even greater preference for *trans,anti* pd[T(A)]=pd[T(A)] between loops 1 and 3 (peak 8) (Fig. S8*C*). These results suggest that the photocrosslinking of G quadruplexes in K^+ is taking place through a highly photoreactive structure other than a triplex, such as the chair or Form III basket, that is in rapid equilibrium with the hybrid structures, and that favors the *trans,anti* dimer between the central Ts of loops 1 and 3.

Conclusion

We have shown that the G-quadruplex form of the human telomere sequence Tel22 is susceptible to both adjacent and interloop-specific thymine photodimer formation in the presence of biologically relevant K^+. The adjacent thymine photodimer has the same *cis,syn* stereochemistry as do the major cyclobutane photodimers induced by UVB light in duplex DNA. The interloop-specific thymine photodimers, however, are all of the *anti* stereochemistry, which is not observed in duplex DNA irradiated under native conditions (16). Thus, *anti* thymine dimers, and in particular their pattern of formation, may represent a unique photochemical signature for the potassium quadruplex form of the human telomeric sequences studied herein, and possibly for other folded DNA structures. Extrapolating from these studies of model systems, we suggest that human telomeric DNA may also be susceptible to UVB-induced *anti* thymine photodimer formation in vivo, in addition to *cis,syn* dimer formation, causing hitherto unrecognized effects on the replication and stability of telomere DNA. Formation of a covalently linked loop of 13–14 nt is also expected to pose a unique challenge to repair systems. It remains to be seen, however, whether *anti* thymine photodimers are produced in human telomere DNA in vivo and if so, how they affect telomere biochemistry. Nuclease P1 coupled LC-MS has been used to detect psoralen photocrosslinks in human genomic DNA (36), but more sensitive ^{32}P-postlabeling assays, or ^{14}C-postlabeling coupled with accelerator mass spectrometry (37), may be required to detect *anti* thymine photodimers in telomeres.

Materials and Methods

Preparation of G-Quadruplexes. Typically, 50 μM ODN (IDT) in 10 mM Tris·HCl, pH 7.5, with 150 mM KCl or NaCl was heated at 95 °C for 5–10 min and then either rapidly cooled down in ice or slowly cooled to room temperature over a couple of hours and then cooled in ice. The formation of G-quadruplexes was confirmed by CD (Fig. S1).

UVB Irradiation. UVB irradiation (270–400 nm with peak intensity at 312 nm) was carried out with two Spectroline XX-15B UV 15-W tubes (rated UV intensity of 1.15 mW/cm^2 at 25 cm) filtered by a LONGLIFE filter (Spectronics Corporation) immediately after sample preparation or after storage at 4 °C for overnight to days with similar results. G-quadruplex samples were enclosed in a polyethylene Ziplock bag and irradiated on a bed of ice for 2–2.5 h at a distance of ≈1 cm from the UVB lamp.

NP1 Digestion. Typically, 1 μL 1 U/μL aqueous NP1 from *Penicillium citrinum* (Sigma) and 1 μL 10 mM $ZnCl_2$ were added to 100 μL 50 μM UVB irradiation samples and digested at 37 °C for >36 h. Digested samples were then converted to the ammonium form for mass spectrometry by mixing with the ammonium form of Dowex resin (Sigma).

HF/Pyridine Hydrolysis. Typically, 8 μL 70% HF/pyridine (Sigma) were added to 15 μg dry NP1 digestion product in a polyethylene microcentrifuge tube and incubated at 37 °C. After 2.5 h, the sample was diluted to 300 μL with Milli-Q water, neutralized with 30 mg calcium carbonate and filtered through an Xpertek 13-mm 0.45-μm nylon syringe filter (P.J. Cobert Associates). The filtrate was evaporated and redissolved in Milli-Q water before HPLC analysis.

HPLC Analysis. Reverse-phase HPLC was carried out with an X-Bridge column (C18, 4.6 × 75 mm, 2.5 μm, 135 Å; Waters Corporation) on a System Gold BioEssential HPLC with a Model 125 binary gradient pump and a Model 168 diode array detector (Beckman Coulter). NP1 digestion products were analyzed with a 1 mL/min gradient of 100% A (50 mM triethylammonium acetate, pH 7.5) for 3 min and 0%–20% B for 3–53 min (50% acetonitrile in 50 mM triethylammonium acetate, pH 7.5) and detected at 260 nm. HF/pyridine hydrolysis products were analyzed with an isocratic gradient of 100% Milli-Q water and detected at 205 nm.

ESI-MS Experiments. Intact/whole-length ODN samples were analyzed in the positive-ion mode on a Waters Micromass Q-Tof Ultima spectrometer. The Z-Spray source was operated at 2.8 kV, the cone voltage was 150 V, and RF lens was 50. The source temperature and desolvation temperatures were 80 ° and 180 °C, respectively. The collision energy was 10 eV, and the MCP detector was 2,200 V. Spray solvent was 30 mM ammonium acetate in 20% methanol. ODNs from NP1-coupled HPLC separation were analyzed in the negative-ion mode with a Thermo Finnigan LTQ-FT mass spectrometer (Thermo Fisher Scientific). A solution of 50/50 (vol/vol) methanol/water was used as the spray solvent. The spray voltage was 3.5 kV. The capillary voltage and temperature were 46 V and 250 °C, respectively. MS/MS experiments were done by using CAD with helium as the collision gas. The mass window for precursor-ion selection was 2.5 *m/z* units. The normalized collision energy (15% of the maximum) was adjusted to obtain product ions of good signal-to-noise ratio. At this setting, nearly all of the precursor ions had fragmented.

ACKNOWLEDGMENTS. We thank Professor Robert Blankenship for use of his CD instrument. This work supported by National Institutes of Health (NIH) Grant CA40463 and Washington University National Institutes of Health Mass Spectrometry Resource Grant 2P41RR000954.

1. Verdun RE, Karlseder J (2007) Replication and protection of telomeres. *Nature* 447:924–931.
2. Gilson E, Geli V (2007) How telomeres are replicated. *Nat Rev Mol Cell Biol* 8:825–838.
3. Riethman H (2008) Human telomere structure and biology. *Annu Rev Genomics Hum Genet* 9:1–19.
4. Patel DJ, Phan AT, Kuryavyi V (2007) Human telomere, oncogenic promoter and 5′-UTR G-quadruplexes: Diverse higher order DNA and RNA targets for cancer therapeutics. *Nucleic Acids Res* 35:7429–7455.
5. Dai J, Carver M, Yang D (2008) Polymorphism of human telomeric quadruplex structures. *Biochimie* 90:1172–1183.
6. Gaynutdinov TI, Neumann RD, Panyutin IG (2008) Structural polymorphism of intramolecular quadruplex of human telomeric DNA: Effect of cations, quadruplex-binding drugs and flanking sequences. *Nucleic Acids Res* 36:4079–4087.
7. Lane AN, Chaires JB, Gray RD, Trent JO (2008) Stability and kinetics of G-quadruplex structures. *Nucleic Acids Res* 36:5482–5515.
8. Wang Y, Patel DJ (1993) Solution structure of the human telomeric repeat d[AG3(T2AG3)3] G-tetraplex. *Structure* 1:263–282.
9. Lim KW, et al. (2009) Structure of the human telomere in K+ solution: A stable basket-type G-quadruplex with only 2 G-tetrad layers. *J Am Chem Soc* 131:4301–4309.
10. Parkinson GN, Lee MP, Neidle S (2002) Crystal structure of parallel quadruplexes from human telomeric DNA. *Nature* 417:876–880.
11. Ambrus A, et al. (2006) Human telomeric sequence forms a hybrid-type intramolecular G-quadruplex structure with mixed parallel/antiparallel strands in potassium solution. *Nucleic Acids Res* 34:2723–2735.
12. Luu KN, Phan AT, Kuryavyi V, Lacroix L, Patel DJ (2006) Structure of the human telomere in K+ solution: An intramolecular (3 + 1) G-quadruplex scaffold. *J Am Chem Soc* 128:9963–9970.
13. Dai J, Carver M, Punchihewa C, Jones RA, Yang D (2007) Structure of the Hybrid-2 type intramolecular human telomeric G-quadruplex in K+ solution: Insights into structure polymorphism of the human telomeric sequence. *Nucleic Acids Res* 35:4927–4940.
14. Phan AT, Kuryavyi V, Luu KN, Patel DJ (2007) Structure of two intramolecular G-quadruplexes formed by natural human telomere sequences in K+ solution. *Nucleic Acids Res* 35:6517–6525.
15. Xu Y, Noguchi Y, Sugiyama H (2006) The new models of the human telomere d[AGGG(TTAGGG)3] in K+ solution. *Bioorg Med Chem* 14:5584–5591.
16. Douki T, Laporte G, Cadet J (2003) Inter-strand photoproducts are produced in high yield within A-DNA exposed to UVC radiation. *Nucleic Acids Res* 31:3134–3142.
17. Su DG, Kao JL, Gross ML, Taylor JS (2008) Structure determination of an interstrand-type cis-anti cyclobutane thymine dimer produced in high yield by UVB light in an oligodeoxynucleotide at acidic pH. *J Am Chem Soc* 130:11328–11337.
18. Xu Y, Tashiro R, Sugiyama H (2007) Photochemical determination of different DNA structures. *Nat Protocols* 2:78–87.
19. Williamson JR, Raghuraman MK, Cech TR (1989) Monovalent cation-induced structure of telomeric DNA: The G-quartet model. *Cell* 59:871–880.
20. Wang Y, Taylor JS, Gross ML (1999) Nuclease P1 digestion combined with tandem mass spectrometry for the structure determination of DNA photoproducts. *Chem Res Toxicol* 12:1077–1082.
21. Gray RD, Chaires JB (2008) Kinetics and mechanism of K+- and Na+-induced folding of models of human telomeric DNA into G-quadruplex structures. *Nucleic Acids Res* 36:4191–4203.
22. Wang Y, Gross ML, Taylor JS (2001) Use of a combined enzymatic digestion/ESI mass spectrometry assay to study the effect of TATA-binding protein on photoproduct formation in a TATA box. *Biochemistry* 40:11785–11793.
23. Volbeda A, Lahm A, Sakiyama F, Suck D (1991) Crystal structure of *Penicillium citrinum* P1 nuclease at 2.8 A resolution. *EMBO J* 10:1607–1618.
24. Romier C, Dominguez R, Lahm A, Dahl O, Suck D (1998) Recognition of single-stranded DNA by nuclease P1: High resolution crystal structures of complexes with substrate analogs. *Proteins* 32:414–424.
25. Henderson E, Hardin CC, Walk SK, Tinoco I Jr, Blackburn EH (1987) Telomeric DNA oligonucleotides form novel intramolecular structures containing guanine-guanine base pairs. *Cell* 51:899–908.
26. Murchie AI, Lilley DM (1994) Tetraplex folding of telomere sequences and the inclusion of adenine bases. *EMBO J* 13:993–1001.
27. Xue Y, et al. (2007) Human telomeric DNA forms parallel-stranded intramolecular G-quadruplex in K+ solution under molecular crowding condition. *J Am Chem Soc* 129:11185–11191.
28. Bose SN, Davies RJH, Sethi SK, McCloskey JA (1983) Formation of an adenine-thymine photoadduct in the deoxydinucleoside monophosphate d(TpA) and in DNA. *Science* 220:723–725.
29. Zhao X, Nadji S, Kao JL-F, Taylor J-S (1996) The Structure of d(TpA)*, the major photoproduct of thymidylyl-(3′-5′)-deoxyadenosine. *Nucleic Acids Res* 24:1554–1560.
30. Cadet J, et al. (1985) Characterization of thymidine ultraviolet photoproducts. Cyclobutane dimers and 5,6-dihydrothymidines. *Can J Chem* 63:2861–2868.
31. Shetlar MD, Basus VJ, Falick AM, Mujeeb A (2004) The cyclobutane dimers of 5-methylcytosine and their deamination products. *Photochem Photobiol Sci* 3:968–979.
32. Li J, Correia JJ, Wang L, Trent JO, Chaires JB (2005) Not so crystal clear: The structure of the human telomere G-quadruplex in solution differs from that present in a crystal. *Nucleic Acids Res* 33:4649–4659.
33. Wang Y, Patel DJ (1995) Solution structure of the *Oxytricha* telomeric repeat d[G4(T4G4)3] G-tetraplex. *J Mol Biol* 251:76–94.
34. Mashimo T, Sannohe Y, Yagi H, Sugiyama H (2008) Folding pathways of hybrid-1 and hybrid-2 G-quadruplex structures. *Nucleic Acids Symp Ser (Oxf)*:409–410.
35. Gray RD, Li J, Chaires JB (2009) Energetics and kinetics of a conformational switch in G-quadruplex DNA. *J Phys Chem B* Jan 5. [Epub ahead of print]
36. Cao H, Hearst JE, Corash L, Wang Y (2008) LC-MS/MS for the detection of DNA interstrand cross-links formed by 8-methoxypsoralen and UVA irradiation in human cells. *Anal Chem* 80:2932–2938.
37. Farmer PB, Singh R (2008) Use of DNA adducts to identify human health risk from exposure to hazardous environmental pollutants: The increasing role of mass spectrometry in assessing biologically effective doses of genotoxic carcinogens. *Mutat Res-Rev Mutat* 659:68–76.